Infrared phonon spectrum of the tetragonal helimagnet $Ba_2CuGe_2O_7$

A. Nucara,[1] W. S. Mohamed,[2] L. Baldassarre,[3] S. Koval,[4] J. Lorenzana,[5] R. Fittipaldi,[6] G. Balakrishnan,[7] A. Vecchione,[6] and P. Calvani[1]

[1]*CNR-SPIN and Dipartimento di Fisica, Università di Roma "La Sapienza", Piazzale A. Moro 2, 00185 Roma, Italy*
[2]*Dipartimento di Fisica, Università di Roma "La Sapienza", Piazzale A. Moro 2, 00185 Roma, Italy*
[3]*Center for Life NanoScience@Sapienza, Istituto Italiano di Tecnologia, Viale Regina Elena 291, 00185 Roma, Italy*
[4]*Instituto de Física Rosario, Universidad Nacional de Rosario, 27 de Febrero 210 Bis, 2000 Rosario, Argentina*
[5]*CNR-ISC and Dipartimento di Fisica, Università di Roma "La Sapienza", Piazzale A. Moro 2, 00185 Roma, Italy*
[6]*CNR-SPIN and Dipartimento di Fisica "E. R. Caianiello", Via Giovanni Paolo II 132, 84084 Fisciano, Salerno, Italy*
[7]*Department of Physics, University of Warwick, Coventry CV4 7AL, United Kingdom*

(Received 15 May 2014; revised manuscript received 8 July 2014; published 23 July 2014)

The lattice dynamics of $Ba_2CuGe_2O_7$, a compound which develops Dzyaloshinsky-Moriya helical magnetism below $T_N = 3.2$ K, has been studied by measuring the infrared reflectivity of a single crystal with the radiation polarized both in the ab plane and along the c axis of its tetragonal cell, from 7 to 300 K. In this compound, where the unit cell has no inversion symmetry, 14 E phonon modes of the ab plane, out of the 18 predicted, and nine B_2 modes of the c axis, out of the ten predicted, have been observed. They have been assigned to the atomic motions by a comparison with shell-model calculations, which provided vibrational frequencies in good agreement with the experiment, while most calculated intensities turned out to be much lower than the experimental values. This discrepancy has been tentatively explained by assuming strong electron-phonon interactions, a hypothesis supported by the failure of the f-sum rule if restricted to the phonon region. Indeed, we observe a remarkable increase in the oscillator strengths between 300 and 200 K for the phonons of the ab plane (between 300 and 100 K for the c axis), which implies an increase in the dielectric constant of $Ba_2CuGe_2O_7$ below room temperature.

DOI: 10.1103/PhysRevB.90.014304 PACS number(s): 78.30.Hv, 63.20.−e

I. INTRODUCTION

Thanks to the growing research effort on the magnetoelectric compounds—which below a critical temperature simultaneously display ferroelectricity and some kind of magnetic order—several mechanisms that can couple magnetism to a macroscopic polarization have been identified. Among them, one of the most interesting is the Dzyaloshinsky-Moriya (DM) effect [1,2], which gives rise to helical spin structures through an exchange Hamiltonian which depends on the vector product between adjacent spins. Such magnetism can also be associated with an electric polarization $\vec{P}$ whose expression contains the same vectorial term [3].

The compound studied here, $Ba_2CuGe_2O_7$ (BCGO), is the only member of the $Ba_2XGe_2O_7$ family which develops helical magnetism at liquid helium temperatures via the DM mechanism [4–6]. Indeed, for $X =$ Mn (spin $S = 5/2$) and Co ($S = 3/2$), the insulator is antiferromagnetic (AF) below Néel temperatures $T_N = 4.0$ and 6.7 K, respectively [3,7,8]. Below T_N, these systems develop a magnetoelectricity due to the spin-dependent hybridization between the d orbitals of the transition metal and the p orbitals of oxygen [9,10]. $Ba_2CuGe_2O_7$, instead, having the Cu^{2+} ion $S = 1/2$, is magnetically much less anisotropic. Below $T_N = 3.2$ K, it thus displays a quasi-AF cycloidal, incommensurate magnetism. However, despite the absence of a center of inversion symmetry in the crystal structure, BCGO does not develop spontaneous ferroelectricity [8]. Nevertheless, a macroscopic electric polarization can be induced in it by an external magnetic field [11].

As the magnetoelectric properties of $Ba_2CuGe_2O_7$ have been extensively discussed in Refs. [3,9,11], the present work is focused on its lattice dynamics, both from an experimental and from a theoretical point of view. We have thus measured the reflectivity $R(\omega)$ of a single crystal of this compound, from 80 to 6000 cm^{-1} and from 7 to 300 K, with the radiation polarized both along the a (or b) axis and along the c axis of the tetragonal unit cell. For both polarizations, the real part $\sigma_1(\omega)$ of the optical conductivity extracted from $R(\omega)$ displays, in the far-infrared region, a number of well-defined phonon peaks, as $Ba_2CuGe_2O_7$ is an excellent insulator. The measured frequencies and intensities have been compared with the predictions of shell-model calculations, which started from the structural determinations by x-ray diffraction. BCGO was found [12] to crystallize in the noncentrosymmetric tetragonal space group $P\bar{4}2_1m$, with lattice parameters $a = b = 0.8466$ nm and $c = 0.5445$ nm. These values are presumably measured at room temperature, and no structural changes induced by temperature are reported in the literature to the best of our knowledge. A schematic view of its unit cell—corresponding to two formula units—is reported in Fig. 1, which reproduces that reported in Ref. [5]. The Ba^{2+} planes, orthogonal to the c axis, separate the layers made of corner-sharing GeO_4 and CuO_4 tetrahedra. It is in the resulting two-dimensional square lattice of Cu^{2+} ions that the Cu spins interact through the DM mechanism and the helical magnetic structure takes place.

II. EXPERIMENT AND RESULTS

Single crystals of $Ba_2CuGe_2O_7$ were grown by the float-zone technique at a pressure of 3 bar in an oxygen gas atmosphere with the growth speed of 0.5 mm/hour [13]. The morphology, phase composition, and purity of the grown crystals were inspected by high-resolution x-ray diffraction and scanning electron microscopy combined with energy

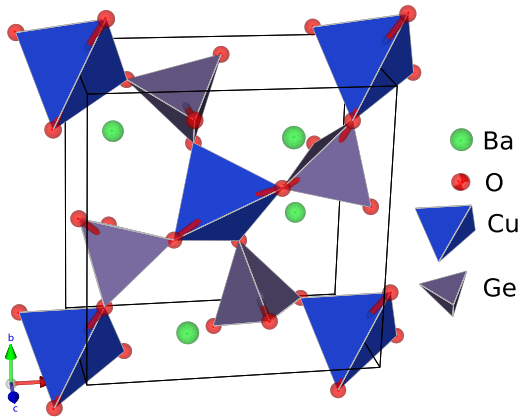

FIG. 1. (Color online) Lattice structure of $Ba_2CuGe_2O_7$ (reelaborated from Ref. [12] with the graphical tools reported in Ref. [14]). The oxygen tetrahedra contain a copper atom if blue and a germanium atom if gray.

dispersive spectroscopy. The crystal orientation was determined by the x-ray back-reflection Laue method showing well-defined, neither distorted nor smeared-out spots. Moreover, the crystals used in this work were cut in such a way that the largest surface contained the a (or b) and the c axes. This surface was finely polished with polycrystalline diamond suspension down to 0.3 μm in grain size, while the orientation of the a-c (or b-c) axes with respect to the sample edges was assessed by the electron back-scattered Kikuchi diffraction technique. The dimensions of the crystals employed in this work were approximately $3 \times 2 \times 1$ mm. In the visible range, they look transparent and colorless, like a piece of glass.

The reflectivity $R(\omega)$ of this surface was measured with a rapid-scanning Michelson interferometer at a resolution of 2 cm^{-1}. Two different polarizations of the radiation field were used: one along the c axis and the other one perpendicular to the c axis (the latter being indicated, in the following, as belonging to the ab plane). The sample was mounted on the cold finger of a helium-flow cryostat. Even if the phonon region is limited to 850 cm^{-1}, $R(\omega)$ was measured by a rapid-scanning interferometer up to 6000 cm^{-1} in order to perform accurate Kramers-Kronig (KK) transformations on it. The reference was a gold film evaporated *in situ* onto the sample. As the crystal is nearly transparent in the midinfrared, to avoid interference fringes its back surface was left unpolished and wedged [15] with respect to the front surface. The real part $\sigma_1(\omega)$ of the optical conductivity was then extracted from $R(\omega)$ by standard KK transforms. The reflectivity was extrapolated to $\omega \to \infty$ by an inverse power law of ω, and to $\omega = 0$ by Lorentzian fits.

The raw reflectivity data of $Ba_2CuGe_2O_7$ are shown in Fig. 2 in the frequency range of interest here, for the radiation polarized both in the ab plane [Fig. 2(a)] and along the c axis [Fig. 2(b)], either at 300 or 7 K. No remarkable effects appear in the spectra at intermediate temperatures, except for an increase in the line intensities that will be discussed below. Both spectra look very similar to the corresponding reflectivity spectra of $Ba_2CoGe_2O_7$, as reported in the same frequency range in Ref. [16]. They are typical of an insulating crystal, with a comb of phonon lines in the far-infrared range, and a

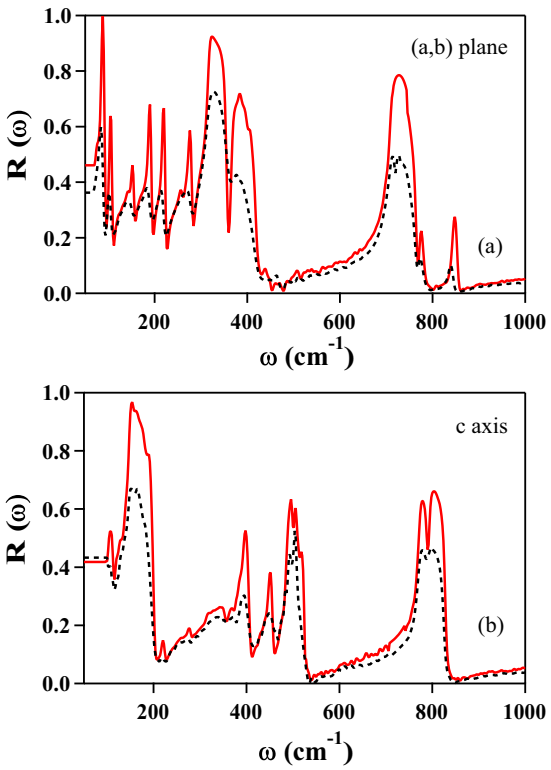

FIG. 2. (Color online) Reflectivity of $Ba_2CuGe_2O_7$ in the far-infrared range of frequencies at 7 K (solid line) and 300 K (dashed line), with the radiation polarized (a) in the ab plane and (b) along the c axis.

flat and very low reflectivity (6–7%) in the midinfrared range (not shown).

The optical conductivity extracted from the data of Fig. 2 is shown for the far-infrared region in Figs. 3(a) and 4(a) for the a,b plane and the c axis, respectively, at two temperatures. The absence of lines common to both polarizations confirms that the polarizer was correctly oriented and that the sample was a single crystal. A factor group analysis predicts for the $P\bar{4}2_1m$ unit cell of $Ba_2CuGe_2O_7$, which includes two formula units, the vibrational representation

$$R = 10A_1 + 6A_2 + 7B_1 + 11B_2 + 19E, \qquad (1)$$

where the E modes are doubly degenerate. One B_2 mode and one E mode are acoustic, the six A_2 modes are silent, and all of the others are optical, Raman-active phonons. Among them, the 18 E and the ten B_2 modes are also infrared active and can be observed with the radiation polarized in the ab plane or along the c axis, respectively. Figures 3(a) and 4(a) show that 14 transverse optical (TO) phonon modes belonging to the ab plane and nine belonging to the c axis could be detected in the present experiment. Their frequencies will be listed in Tables II and III, respectively.

III. SHELL-MODEL CALCULATIONS

In order to understand the complex phonon spectrum of BCGO, we have used a shell model (SM), which enabled us to perform lattice dynamical calculations and to compare the results with the measured $\sigma_1(\omega)$. The SM has been successfully

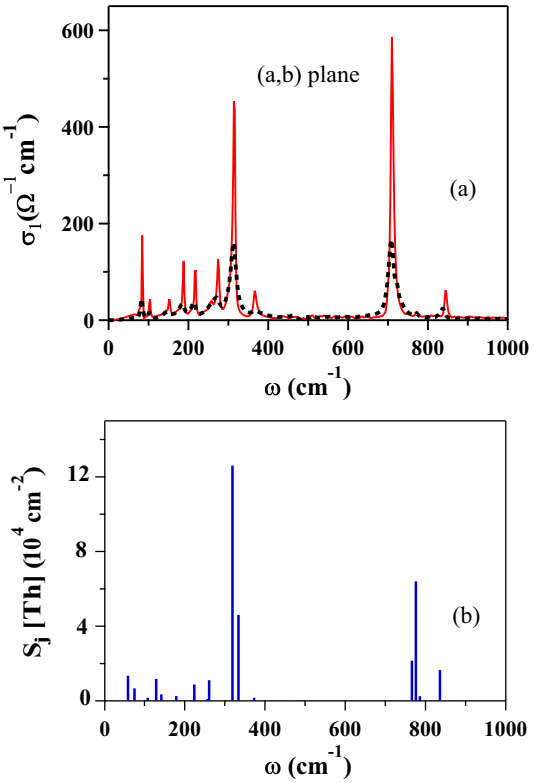

FIG. 3. (Color online) (a) Optical conductivity of $Ba_2CuGe_2O_7$, in the far-infrared range of frequencies at 7 K (solid line) and 300 K (dashed line), with the radiation polarized in the *ab* plane. b) Shell-model results for the vibrational modes of the *ab* plane. The bar length is the calculated strength $S_{j\text{th}}$ in cm^{-2}.

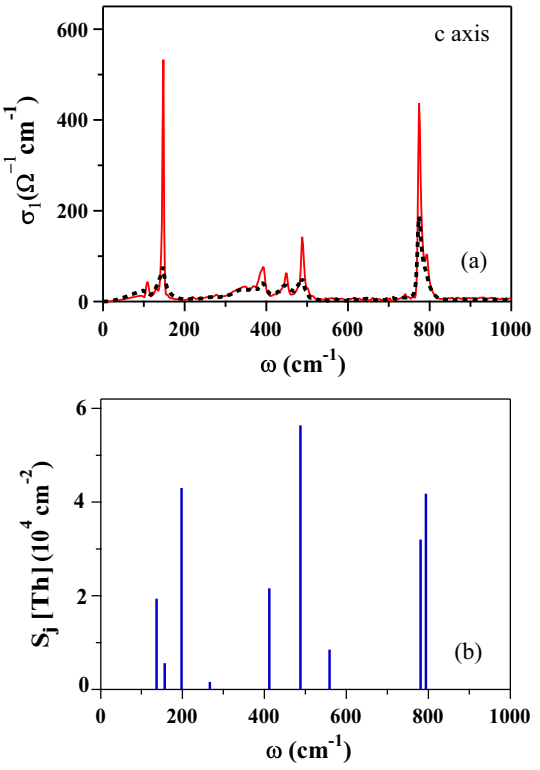

FIG. 4. (Color online) (a) Optical conductivity of $Ba_2CuGe_2O_7$ in the far-infrared range of frequencies at 7 K (solid line) and 300 K (dashed line), with the radiation polarized along the *c* axis. (b) Shell-model results for the vibrational modes along the *c* axis. The bar length is the calculated strength $S_{j\text{th}}$ in cm^{-2}.

applied to different compounds (oxides and hydrides) where the effects of the anion polarizability turned out to be important for a proper description of the vibrational properties [17–20]. The ionic polarizability is taken into account by considering electronic shells with charge Y coupled harmonically by a force constant k to an atomic core. The SM includes long-range Coulomb interactions between all charged shells and cores, and shell-shell short-range interactions arising from the wave-function overlap between neighboring ions. We have considered short-range interactions of the Born-Mayer type, $A\exp(-\frac{r}{\rho})$, for the Cu-O, Ba-O, and Ge-O bonds. The lattice constants and the atomic positions were taken from the experimental data of Ref. [12].

To calculate the oscillator frequencies and strengths, we have fixed the total charges Z of the ions to their nominal values, i.e., $Z_O = -2$, $Z_{Cu} = 2$, $Z_{Ba} = 2$, and $Z_{Ge} = 4$. The model contains 14 adjustable parameters. The initial parameter values were taken from Refs. [21,22] and were subsequently modified in order to fit the measured infrared phonon frequencies at the Brillouin-zone center. The calculations were carried out with the help of the GULP code [23]. Due to the complexity of the structure and consequently of the developed SM, the use of automatic searches for parameters included in the code turned out to be ineffective [20]. Thus, the adjustment of the parameters was made by hand. The final set of SM parameters which gave the best fit to data is shown in Table I. An important effect of the ionic polarizabilities is that they modify the oscillator strengths of the optical absorption, an effect that is often accounted for by using the concept of Born effective charges.

The theoretical frequencies $\Omega_{j\text{th}}$ of the transverse optical (TO) infrared phonons obtained with the model are shown in Table II for the *ab* plane and in Table III for the *c* axis. Also shown are the calculated oscillator strengths $S_{j\text{th}}$ for each jth TO infrared mode [23,24]. The resulting components of the dielectric function tensor, which is diagonal here and also symmetric in the *ab* plane, are reported in Table IV in both limits of zero frequency and high frequency.

IV. COMPARISON BETWEEN THEORY AND EXPERIMENT

In Tables II and III, the theoretical frequencies and oscillator strengths of the phonon modes are compared with the

TABLE I. Shell-model potential parameters (A,ρ), shell charges (Y), and on-site core-shell force constants (k).

Interaction	A (eV)	ρ (Å)	Ion	Y (e)	k (eV/Å^2)
Ba-O	915	0.397	Ba	-2	251
Cu-O	900	0.305	Cu	4	175
Ge-O	3000	0.280	Ge	0	1000
			O	-2.59	50

TABLE II. The *ab* plane calculated phonon frequencies $\Omega_{j\text{th}}$ and oscillator strengths $S_{j\text{th}}$ are compared with the frequencies Ω_j, oscillator strengths S_j, and widths Γ_j, obtained by fitting to Eq. (2) the experimental $\sigma_1(\omega)$ at 7 and 300 K. Ω_j and Γ_j are given in cm^{-1}; S_j is given in cm^{-2}.

Phonon (j)	$\Omega_{j\text{th}}$	Ω_j (7 K)	Ω_j (300 K)	$S_{j\text{th}}$	S_j (7 K)	S_j (300 K)	Γ_j (7 K)	Γ_j (300 K)
1	59			13400				
2	75	84	82	6700	27000	12500	2	5
3	108	103	102	1700	8000	2300	2	3
4	129			11800				
5	142	152	146	3500	14500	9500	7.5	15
6	179	187	182	2600	30000	26500	4	18
7	224	217	212	8750	26000	19000	4	11
8	258	257	258	970	33000	32000	21	25
9	261	274	270	11100	40000	22600	6	15
10	319	310	305	126000	89000	39000	11	20
11	334	315	313	46000	111000	120000	4	15
12	374	367	371	1700	26000	17000	8	30
13	443			30				
14	489			450				
15	766	710	707	21500	213000	153000	7	17
16	776	714	724	64000	64000	42000	10	23
17	786	772	772	2500	5300	3000	8	8
18	836	844	838	16500	24000	12000	7	10

corresponding values obtained by fitting to the experimental optical conductivity the Lorentzian expression

$$\sigma_1(\omega) = \frac{1}{60}\sum_{j=1}^{n}\frac{\omega^2\Gamma_j S_j}{\left(\Omega_j^2-\omega^2\right)^2+\omega^2\Gamma_i^2}. \qquad (2)$$

In Eq. (2), $\sigma_1(\omega)$ is measured in $\Omega^{-1}\,\text{cm}^{-1}$, while Ω_j and Γ_j are the central frequency, and the linewidth of the jth transverse optical mode, respectively, in cm^{-1}. S_j is the oscillator strength in cm^{-2}.

The atomic displacements for selected phonons of the *ab* plane are shown in Fig. 5. They are labeled by their number in Table II and by the theoretical frequency in cm^{-1} (also, see Supplemental Material [25]). Surprisingly, we find that in many modes, the CuO tetrahedra and the GeO tetrahedra have a similar pattern, and this is the case of the four modes shown in Fig. 5. This behavior is probably due to the similarity of the Ge and the Cu mass which makes the tetrahedral "molecules" vibrate at similar frequencies and appreciably mix their modes in the solid. Therefore, we shall discuss the pattern by referring to the tetrahedra without specifying the central atom.

In the 129 cm^{-1} mode [Fig. 5(a)], the atom at the center of the tetrahedra and three vertex oxygens move approximately in the same direction, while a fourth vertex oxygen moves in a quasiperpendicular direction. Thus the angle of only one Cu-O (or Ge-O) bond is significantly perturbed. In the 224 cm^{-1} mode [Fig. 5(b)], two oxygens move approximately parallel to the central atom and two others move in a quasiopposite direction, causing a larger distortion of the tetrahedra even if, again, mainly in the internal angles. In the 319 cm^{-1} mode [Fig. 5(c)], the pattern is again similar for the Cu and Ge tetrahedra but they move out of phase. The central Cu moves toward a vertex O when the central Ge moves away from a vertex O. As the other atoms move perpendicular to the

TABLE III. The *c*-axis calculated phonon frequencies $\Omega_{j\text{th}}$ and oscillator strengths $S_{j\text{th}}$ are compared with the frequencies Ω_j, oscillator strengths S_j, and widths Γ_j, obtained by fitting to Eq. (2) the experimental $\sigma_1(\omega)$ at 7 and 300 K. Ω_j and Γ_j are given in cm^{-1}; S_j is given in cm^{-2}.

Phonon (j)	$\Omega_{j\text{th}}$	Ω_j (7 K)	Ω_j (300 K)	$S_{j\text{th}}$	S_j (7 K)	S_j (300 K)	Γ_j (7 K)	Γ_j (300 K)
1	137	109	100	19400	17000	24000	7	22
2	157	130	131	5600	6500	7500	5	10
3	198	147	146	43000	121000	66000	3	16
4	267	278	269	1600	1900	3300	4	19
5	318	321	320	100	700	300	10	12
6	412	390	391	21600	58000	30000	15	19
		448	446		36000	43000	11	27
7	488	488	485	56400	74000	47000	9	18
8	559			8500				
9	781	775	771	32000	174000	91000	7	9
10	794	791	786	41800	84000	81000	17	21

TABLE IV. Calculated values of the dielectric constant ϵ_0 and of the high-frequency dielectric function ϵ_∞ in the *ab* plane and along the *c* axis.

ϵ_0^{ab}	ϵ_0^{c}	ϵ_∞^{ab}	ϵ_∞^{c}
10.34	4.67	1.96	1.77

bonds, they mainly change their angles, causing the mode to be a mixture of bending and stretching. This explains its relatively large energy. The 776 cm^{-1} mode [Fig. 5(d)] has a stronger stretching character, as shown by its high energy, although one never finds in BCGO either purely stretching or purely bending modes, as is the case in higher-symmetry solids. This also explains why here, at variance with many oxides where the highest vibrational frequency corresponds to a pure oxygen stretching mode, the highest-energy lines do not shift appreciably when decreasing the temperature.

Finally, Fig. 6 shows selected phonon modes polarized along the *c* axis. They are labeled by their number in Table III and theoretical frequency in cm^{-1} [25]. The mode [Fig. 6(a)] at 137 cm^{-1} shows a rigid motion of the Cu tetrahedra with the Ba in antiphase. The Ge ions practically do not move and act as "nodes" of the vibration. In most other modes, instead, the two kinds of tetrahedra show very similar displacements, as discussed above for the *ab* plane. In the mode [Fig. 6(b)] at 198 cm^{-1}, the Cu and Ge tetrahedral "molecules" move in antiphase and the Ba ions have smaller displacements. The mode [Fig. 6(c)] at 488 cm^{-1} is a mixture of stretching and bending, similar to the mode of Fig. 5(c). Finally, in the mode [Fig. 6(d)] at 794 cm^{-1}, the stretching character of the bonds bridging the O's to the center of the tetrahedra prevails.

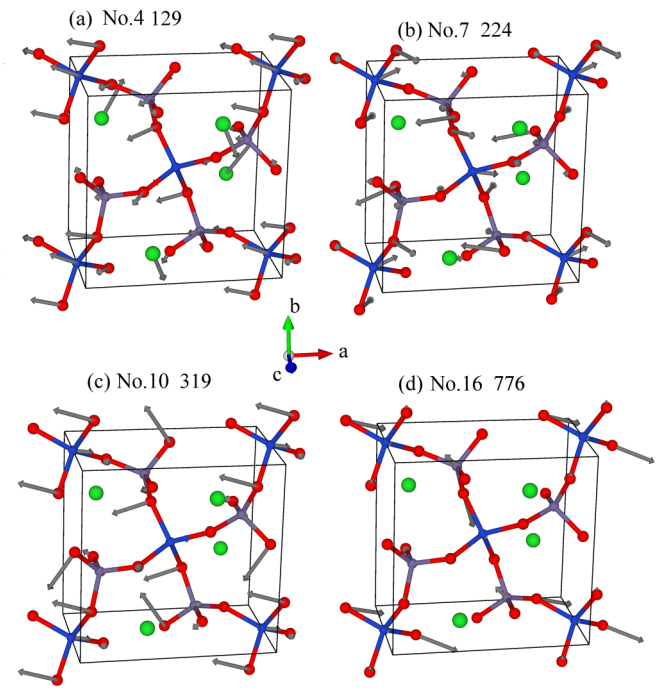

FIG. 5. (Color online) Atomic displacements for selected phonon modes of $Ba_2CuGe_2O_7$ in the *ab* plane. Each mode is identified by its number in Table II and by its calculated frequency, in cm^{-1} [25].

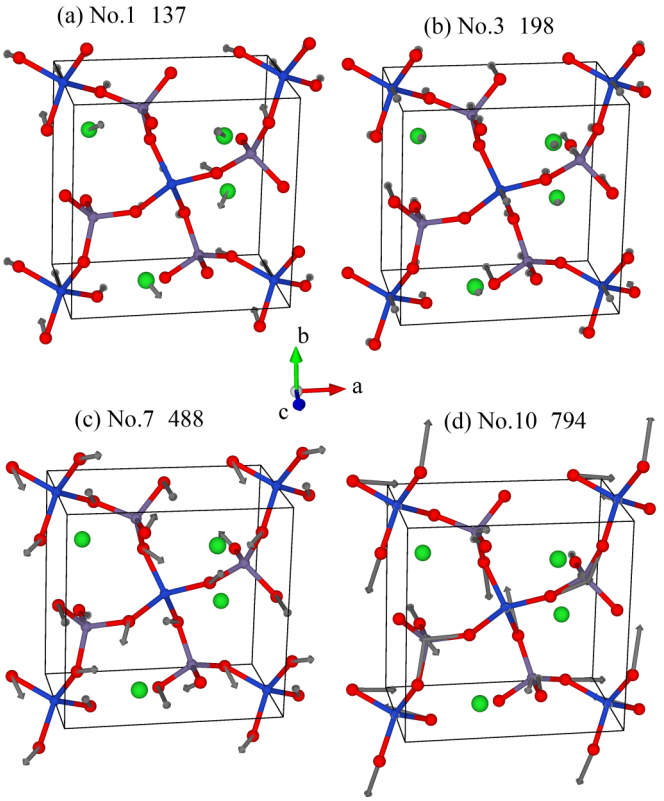

FIG. 6. (Color online) Atomic displacements for selected modes of $Ba_2CuGe_2O_7$ along the *c* axis. Each mode is identified by its number in Table III and by its calculated frequency, in cm^{-1} [25].

As one can see in Tables II and III, as well as in Figs. 3 and 4, there is a good agreement—within the experimental linewidths—between the observations and the theoretical predictions, as far as the phonon frequencies are concerned. The main discrepancies concern phonons 15 and 16 of the *ab* plane and modes 1–3 of the *c* axis, where the calculated frequencies are much higher than the observed ones. This may be ascribed either to anharmonic effects which particularly affect those modes, not taken into account in the model, or to an overestimation of the shell-shell repulsive interactions. The latter problem may be specifically present in the Cu-O and/or Ge-O bonds in the case of the *ab*-polarized phonons 15 and 16, and in the Ba-O bond in the case of the *c*-polarized modes 1–3. Moreover, four modes of the *ab* plane were not observed: mode 1 is out of the measuring range, 13 and 14 are too weak, while modes 4 and 5 are probably unresolved, as one can see by comparing their total intensity with the intensity of the observed line. In the spectrum of the *c* axis, the bump at 448 cm^{-1}, not predicted by the theory, might be a shoulder of the closest mode 7, while mode 8 was not resolved. Concerning the oscillator strengths, most calculated values reported in the same tables and figures match the order of magnitude of those measured in the real system, but are systematically lower. This may be mainly due to the so-called charged-phonon effect [26], by which phonons acquire an anomalously large spectral weight due to interatomic movement of charge associated with

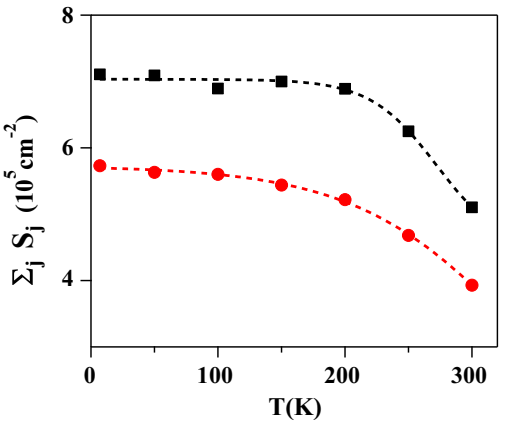

FIG. 7. (Color online) The total oscillator strength of the phonons polarized in the ab plane of $Ba_2CuGe_2O_7$ (squares) and along its c axis (circles) is plotted vs temperature. The lines are guides to the eye.

their displacement pattern. Such effect is not included in the shell model, which only takes into account on-site distortions of the atomic cloud. This results in a transfer of spectral weight to the far-infrared region from the electronic bands in the near-infrared and the visible region. Similar "dressed phonons" were observed in several perovskites with high polarizability [27,28] through a strong increase of the phonon intensities at low temperature, especially for the lowest-frequency modes, and through the failure of the f-sum rule,

$$\int_{\mathrm{FIR}} \sigma(\omega,T)d\omega = \mathrm{const}, \tag{3}$$

when, as in Eq. (3), it is restricted to the far-infrared (FIR) region. Indeed, in $Ba_2CuGe_2O_7$, both the O and Cu ions are largely polarizable as shown by the large shell charges and the small core-shell force constants (see Table I) required by the model fitting of the observed spectra. We therefore compared with each other the intensities provided by the fits at the lowest and highest temperatures of the experiment. As shown in Tables II and III, most phonons are more intense at low temperature, so that $\sum_j S_j$ (7 K) is larger than $\sum_j S_j$ (300 K) by about 40% for the ab plane and 45% for the c axis. This effect, which "dresses" the phonons, is not taken into account in the shell model employed here, and may explain most of the discrepancies between theory and experiment which emerge in Tables II and III. The f-sum-rule violation also has the interesting implication that the dielectric constant of $Ba_2CuGe_2O_7$, which is related to $\sum_j S_j$ [27], is higher than the theoretical values in Table IV and should also increase when cooling the system below room temperature. As is shown in Fig. 7, the phonon strengthening for decreasing temperature saturates around 200 K for the ab plane and around 100 K for the c axis: in both cases, at $T \gg T_N$. Moreover, it occurs gradually and without any discontinuity, which may suggest a transition of any sort.

V. CONCLUSION

In the present work, we have studied the lattice dynamics of $Ba_2CuGe_2O_7$ by infrared reflectivity measurements with polarized radiation, down to temperatures close to those where a helimagnetic phase takes place via the Dzyaloshinsky-Moriya mechanism. The number of the observed phonon lines is lower than that predicted for the $P\bar{4}2_1m$ cell of $Ba_2CuGe_2O_7$, and no line splitting has been observed when cooling the sample to 7 K. Therefore, our spectra confirm that the tetragonal symmetry is conserved down to the lowest temperatures above T_N, with no appreciable distortion. The optical conductivity extracted from $R(\omega)$ has been fit by a sum of Lorentzians, and their parameters have been compared with the results of shell-model calculations. These have correctly predicted the observed frequencies, within the experimental linewidths, except for a few modes where the theoretical values are systematically higher. The discrepancy may be due either to anharmonic effects, not taken into account in the model, or to an overestimation of the shell-shell repulsive interactions. A systematic underestimation with respect to the observed values is instead exhibited by the calculated oscillator strengths. We have tentatively explained this effect by considering that "charged-phonon" effects—not considered in the model—can increase the dipole moment of those vibrations due to the distortion of the electron clouds going beyond one atom. Such interpretation is consistent both with the strong increase observed in the phonon intensities for decreasing temperature and with the failure of the optical sum rule when it is restricted to the phonon region. Although we cannot make a quantitative estimate because of lack of experimental information in the terahertz region and below, the remarkable increase in the phonon intensities that we observe at temperatures much higher than T_N suggests that the dielectric constant of $Ba_2CuGe_2O_7$ may increase below room temperature for a redistribution of the electric charge within the cell. Measurements of the static dielectric constant could verify this expectation.

ACKNOWLEDGMENTS

This work has been partially supported by the 2012 and 2013 Ateneo grants of Università di Roma La Sapienza. We thank Paolo Barone for suggesting software tools useful for the figure preparation. S.K. thanks J. Gale and R. Migoni for useful discussions, and acknowledges support from the Consejo Nacional de Investigaciones Científicas y Técnicas de la República Argentina. G.B. thanks EPSRC, UK for funding this work at the University of Warwick.

[1] I. E. Dzyaloshinskii, J. Phys. Chem. Solids **4**, 241 (1958).
[2] T. Moriya, Phys. Rev. **120**, 91 (1960).
[3] H. Murakawa, Y. Onose, S. Miyahara, N. Furukawa, and Y. Tokura, Phys. Rev. B **85**, 174106 (2012).
[4] A. Zheludev, G. Shirane, Y. Sasago, N. Koide, and K. Uchinokura, Phys. Rev. B **54**, 15163 (1996).
[5] A. Zheludev, S. Maslov, G. Shirane, Y. Sasago, N. Koide, and K. Uchinokura, Phys. Rev. B **57**, 2968 (1998); A. Zheludev, S. Maslov, G. Shirane, I. Tsukada, T. Masuda, K. Uchinokura, I. Zaliznyak, R. Erwin, and L. P. Regnault, *ibid.* **59**, 11432 (1999).
[6] J. Chovan, M. Marder, and N. Papanicolaou, Phys. Rev. B **88**, 064421 (2013).

[7] T. Masuda, S. Kitaoka, S. Takamizawa, N. Metoki, K. Kaneko, K. C. Rule, K. Kiefer, H. Manaka, and H. Nojiri, Phys. Rev. B **81**, 100402(R) (2010).
[8] A. Zheludev, T. Sato, T. Masuda, K. Uchinokura, G. Shirane, and B. Roessli, Phys. Rev. B **68**, 024428 (2003).
[9] H. Murakawa, Y. Onose, S. Miyahara, N. Furukawa, and Y. Tokura, Phys. Rev. Lett. **105**, 137202 (2010).
[10] K. Yamauchi, P. Barone, and S. Picozzi, Phys. Rev. B **84**, 165137 (2011).
[11] H. Murakawa, Y. Onose, and Y. Tokura, Phys. Rev. Lett. **103**, 147201 (2009).
[12] M. Tovar, R. E. Dinnebier, and W. Eysel, Mater. Sci. Forum **278-281**, 750 (1998).
[13] R. Fittipaldi, G. Balakrishnan, and A. Vecchione (unpublished).
[14] K. Momma and F. Izumi, J. Appl. Crystallogr. **44**, 1272 (2011).
[15] P. Dore, A. Nucara, D. Cannavó, G. De Marzi, P. Calvani, A. Marcelli, R. S. Sussmann, A. J. Whitehead, C. N. Dodge, A. J. Krehan, and H. J. Peters, Appl. Opt. **37**, 5731 (1998).
[16] V. Hutanu, A. Sazonov, M. Meven, H. Murakawa, Y. Tokura, S. Bordács, I. Kézsmárki, and B. Náfrádi, Phys. Rev. B **86**, 104401 (2012).
[17] S. Koval, R. Migoni, and H. Bonadeo, J. Phys.: Condens. Matter **4**, 4759 (1992).
[18] S. Koval, M. G. Stachiotti, R. L. Migoni, M. S. Moreno, R. C. Mercader, and E. L. Peltzer y Blancá, Phys. Rev. B **54**, 7151 (1996).
[19] J. Lasave, F. Dominguez, S. Koval, M. G. Stachiotti, and R. L. Migoni, J. Phys.: Condens. Matter **17**, 7133 (2005).
[20] J. Lasave, J. Kohanoff, R. L. Migoni, and S. Koval, Physica B **404**, 2736 (2009).
[21] M. Braden, W. Reichardt, B. Hennion, G. Dhalenne, and A. Revcolevschi, Phys. Rev. B **66**, 214417 (2002).
[22] S. Tinte, M. G. Stachiotti, M. Sepliarsky, R. L. Migoni, and C. O. Rodriguez, J. Phys.: Condens. Matter **11**, 9679 (1999).
[23] J. D. Gale, J. Chem. Soc. Faraday Trans. **93**, 629 (1997).
[24] S. Koval and R. Migoni, Phys. Rev. B **51**, 6634 (1995).
[25] See Supplemental Material at http://link.aps.org/supplemental/10.1103/PhysRevB.90.014304 for similar figures for all of the other infrared-active phonons of the *ab* plane and the *c* axis.
[26] M. J. Rice, Solid State Commun. **31**, 93 (1979).
[27] C. C. Homes, T. Vogt, S. M. Shapiro, S. Wakimoto, and A. P. Ramirez, Science **293**, 673 (2001).
[28] C. C. Homes, T. Vogt, S. M. Shapiro, S. Wakimoto, M. A. Subramanian, and A. P. Ramirez, Phys. Rev. B **67**, 092106 (2003).